Journal of ELECTRONIC MATERIALS, Vol. 40, No. 3, 2011
DOI: 10.1007/s11664-010-1488-6

An Investigation of Diffusion Barrier Characteristics of an Electroless Co(W,P) Layer to Lead-Free SnBi Solder

HUNG-CHUN PAN[1] and TSUNG-EONG HSIEH[1,2]

1.—Department of Materials Science and Engineering, National Chiao Tung University, 1001 Ta-Hseuh Road, Hsinchu 30010, Taiwan, ROC. 2.—e-mail: tehsieh@mail.nctu.edu.tw

Diffusion barrier characteristics for eutectic SnBi solder/electroless Co(W,P) couples were investigated via liquid-state aging at 250°C and solid-state aging at 120°C. At the couple interface, $CoSn_3$ intermetallic compound (IMC) spallation was observed for the SnBi/amorphous Co(W,P) couple subjected to liquid-state aging. In contrast, no spallation of IMCs was observed for the SnBi/amorphous Co(W,P) couples subjected to solid-state aging. For the SnBi/polycrystalline Co(W,P) couple, a thick IMC layer was observed adjacent to a tungsten-enriched amorphous interfacial layer regardless of aging conditions. IMC formation in all samples indicated that Co(W,P) is essentially a sacrificial barrier to SnBi solder. However, amorphous Co(W,P) might also exhibit stuffed-type barrier behavior due to its relatively high phosphorus (P) content. Analytical results indicated that the P content in Co(W,P) is a crucial factor affecting the structural evolution at the SnBi/electroless Co(W,P) interface.

Key words: Diffusion barrier, electroless Co(W,P), lead-free SnBi solder, intermetallic compounds

INTRODUCTION

Diffusion barriers are important components in solder connections to prevent undesired alloy reactions that may degrade the performance of electronic devices. For instance, flip-chip (FC) bonding requires an under bump metallurgy (UBM), which is a multilayer structure comprising an adhesion layer, a diffusion barrier layer, and a passivation layer. The UBM inhibits interdiffusion between the solder bump and the integrated circuit (IC) bond pad material to ensure reliable IC operation. Diffusion barriers are classified as sacrificial, stuffed, passive compound, and amorphous type according to the principle of diffusion inhibition.[1] Refractory metals such as tungsten (W) and molybdenum (Mo), and their alloys, are common barrier layers in UBMs, and they are usually prepared by physical vapor deposition processes such as e-beam evaporation or sputter deposition. Recently, electroless plating technology, e.g., electroless nickel (EN), has become a popular alternative due to its low cost, high process throughput, high corrosion resistance, good step coverage, etc. In addition to the slower reaction rate of Ni-based UBMs with solders, in comparison with Cu-based UBMs,[2] the satisfactory barrier properties of amorphous EN layers are ascribed to the lower film stresses in comparison with sputtered Ni[3] and the absence of fast-diffusion grain boundaries in amorphous EN films.[4–7]

Eutectic SnBi ($Sn_{43}Bi_{57}$, eutectic point 138°C) is an important low-temperature lead-free solder. Alloy reactions between SnBi and EN or Cu layers and their barrier characteristics have been extensively studied.[8–18] Recently, electroless cobalt (Co) has attracted a lot of research interest due to its promising application as a diffusion barrier in Cu-ICs[19] and UBMs.[20–23] However, studies regarding the diffusion barrier characteristics of electroless Co layer/SnBi solder couples are lacking. In this work, we prepared electroless cobalt-tungsten-phosphorus [Co(W,P)] layers, either amorphous or polycrystalline, and studied their diffusion barrier properties relative to deposited eutectic SnBi solder. The experiments included both liquid-state aging at 250°C up to 5 h and solid-state aging at 120°C up to 1000 h. The microstructures at the solder/Co(W,P)

(Received July 19, 2010; accepted December 6, 2010; published online January 5, 2011)

interface were evaluated at different aging times, and the corresponding diffusion barrier mechanisms are presented herein.

EXPERIMENTAL PROCEDURES

Silicon (Si) wafers sequentially coated with 50-nm-thick Ti and 100-nm-thick Cu layers were adopted as the substrates for this study. Ti serves as the adhesion layer, while Cu simulates the metal interconnection in Cu-ICs. Pretreatments including roughening, sensitization, and activation were carried out first. The chemicals and processing conditions for pretreatments and electroless plating are listed in Tables I and II. Then an about 6-μm- to 7-μm-thick electroless Co(W,P) layer was deposited on the substrates. During the electroless deposition, the *V/A* ratio (the ratio of plating solution volume to the plating surface area in units of mL/cm^2) was adjusted to be ≥50. The plating bath pH value was monitored by a pH meter and adjusted by using KOH solution so that a Co(W,P) layer with the desired crystallinity could be achieved. Amorphous Co(W,P) was prepared at pH 8.6, while polycrystalline Co(W,P) was obtained at pH 7.6. Under such processing conditions, amorphous Co(W,P) with a phosphorus (P) content of approximately 9 at.% to 10 at.% and a tungsten (W) content of 1 at.% or polycrystalline Co(W,P) with a P content of ~4 at.% and a W content of ~8 at.% was obtained. After the electroless deposition, an appropriate amount of eutectic SnBi solder paste (PF602-P, lot no. 0802002; Shenmao Technology Inc.) was immediately applied on the Co(W,P), and a brief reflow treatment at 250°C for 30 s was carried out to solidify the solder. Afterwards, the samples were vacuum-sealed, transferred to the furnace, and heated either at 250°C for liquid-state aging up to 5 h or at 120°C for solid-state aging up to 1000 h. Note that the liquid-state aging was performed at a temperature somewhat higher than the melting point of SnBi. This facilitated the alloy reactions so that the microstructure evolution at the reacting interface could be easily observed. Field-emission scanning electron microscopy (FE-SEM; FEI Quanta 400F or JSM-6500F) and transmission electron microscopy (TEM, Tecnai F-20; Philips) in conjunction with energy-dispersive spectroscopy (EDS; Genesis) were used to investigate the microstructure and composition changes in the specimens. The cross-sectional TEM (XTEM) samples were prepared by focused ion beam (FIB; FEI-201) technique supported by Materials Analysis Technology, Inc., Chupei, Taiwan, ROC.

Table I. Chemicals and processing conditions of pretreatment

Step	Component	Concentration	Immersion Time
Roughening	H_2SO_4	5 wt.%	30 s
Sensitization	$SnCl_2{\cdot}2H_2O$	10 g/L	5 min
	HCl	40 mL/L	
Activation	$PdCl_2{\cdot}2H_2O$	10 g/L	1 min
	HCl	40 mL/L	

Table 2. Chemicals and processing conditions of electroless Co(W,P) plating

Component		Concentration (g/L)
Co source	$CoSO_4{\cdot}7H_2O$	23
Reducing agent	$NaH_2PO_2{\cdot}H_2O$	18
Complexing agent	Na_3 citrate	144
Buffer agent	H_3BO_3	31
W source	$Na_2WO_4{\cdot}2H_2O$	10
pH value		7.6 or 8.6
Temperature		90°C

RESULTS AND DISCUSSION

SnBi/Amorphous Co(W,P) Samples

Liquid-State Aging

Figure 1a–d depict cross-sectional SEM micrographs of SnBi/amorphous Co(W,P) samples subjected to liquid-state aging for 1 min, 20 min, 30 min, and 1 h, respectively. At the beginning of heat treatment (Fig. 1a), thin lath-like Co-Sn intermetallic compounds (IMCs) grew out from the SnBi/Co(W,P) interface into the solder, whereas isolated reaction zones formed in the Co(W,P) region. As the aging time increased, the IMCs coarsened to thick platelets and the isolated reaction zones coalesced to a continuous reaction layer, as illustrated in Fig. 1b. In the meantime, the IMCs partially spalled away from the reacting interface. After 30 min liquid-state aging, most IMCs spalled into the solder and an approximately 500-nm-thick reaction layer formed between the solder and Co(W,P), as shown in Fig. 1c. As shown in Fig. 1d, almost all the IMCs spalled away from the reaction interface when the aging time was extended to 1 h. Formation of IMCs revealed by SEM analysis indicated that an amorphous Co(W,P) film was a sacrificial-type barrier to SnBi solder, so it is important that the Co(W,P) layer is sufficiently thick to prevent complete dissolution into the SnBi solder.

EDS analysis indicated the Co-to-Sn ratio in the lath-like IMCs to be about 1:3 to 1:4. Furthermore, about 3 at.% to 4 at.% of Bi was frequently detected in the IMCs. In view of the inaccuracy of EDS spatial detection, the IMCs are most likely of $CoSn_3$ type doped with a small amount of Bi, since Bi is partially soluble in Sn-rich alloy.[24] The reaction layer in between the solder and the Co(W,P) was found (by EDS) to comprise various elements, e.g., Co, Sn, P, W, and Bi, with a P content as high as 15 at.% and a tungsten (W) content of about 2.25 at.%. The increased P and W contents are

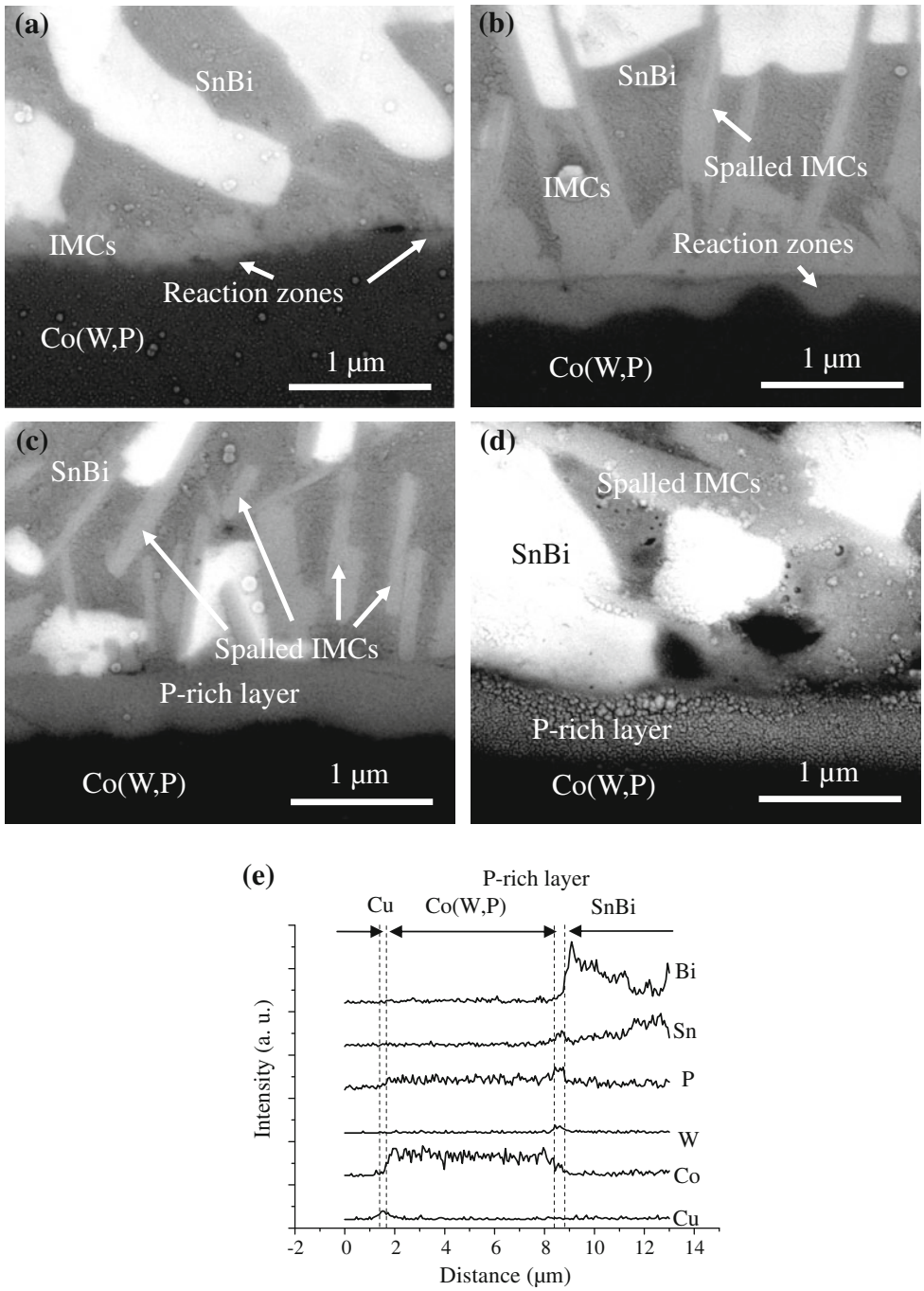

Fig. 1. SEM micrographs of SnBi/amorphous Co(W,P) samples subjected to liquid-state aging for (a) 1 min, (b) 20 min, (c) 30 min and (d) 1 h. (e) EDS line scan profiles corresponding to the sample shown in (d).

ascribed to the accumulation of P and W at the reaction interface when Co is consumed by Sn to form the $CoSn_3$ IMCs. Owing to its high P content, the reaction layer is hereinafter termed the P-rich layer.

Figure 1e depicts EDS line scan profiles for the 1-h-aged samples shown in Fig. 1d. In conjunction with the TEM analysis presented below, the absence of Cu and Sn signals in the unreacted Co(W,P) implies that Co(W,P) may also serve as a stuffed-type diffusion barrier to the Cu underlayer due to the supersaturation by P as well as the fine Co_2P IMCs dispersed in the Co(W,P). Hence, amorphous Co(W,P) is a mixed-type barrier applied to joints containing SnBi solder.

Previous SEM characterization revealed that the P-rich layer seems to not thicken significantly after 30 min aging. To verify this, we performed liquid-state aging up to 5 h, and the corresponding SEM images are presented in Fig. 2a, b. It can be seen

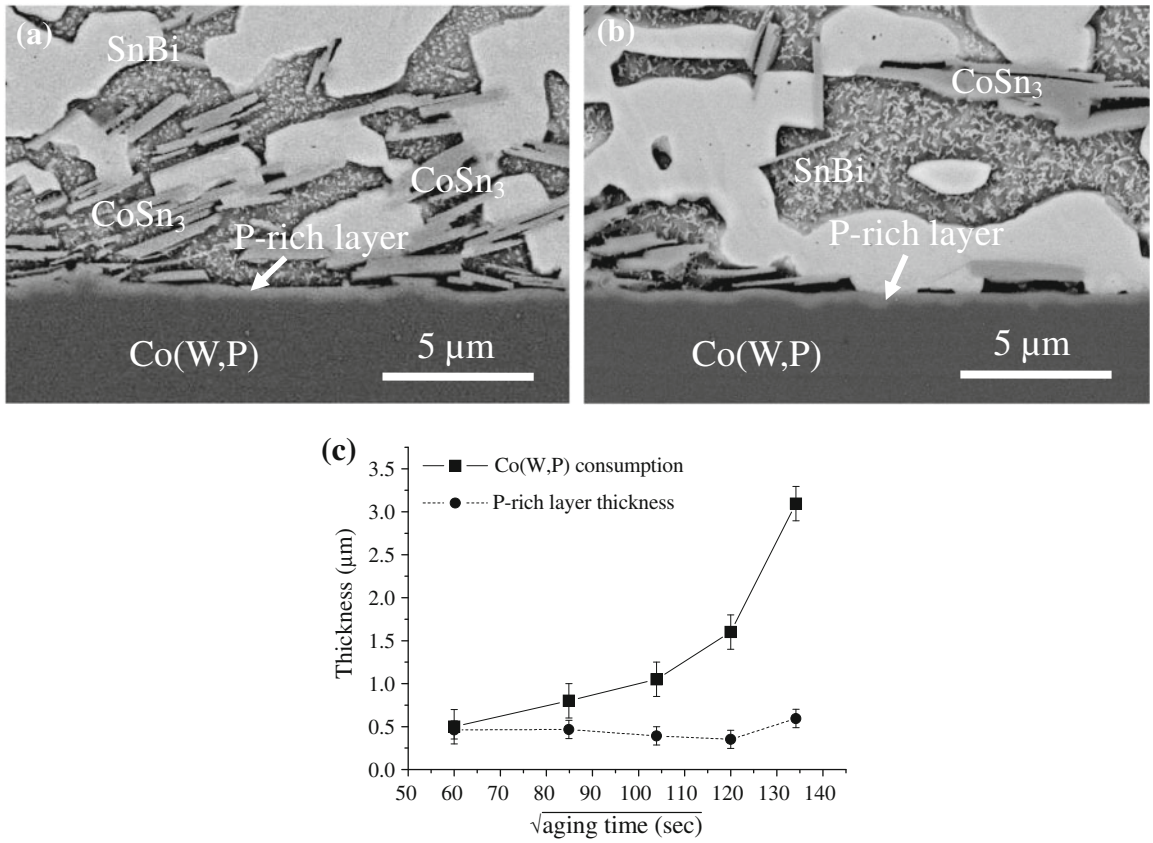

Fig. 2. Cross-sectional SEM view of SnBi/amorphous Co(W,P) sample subjected to liquid-state aging for (a) 2 h and (b) 5 h. (c) Thicknesses of the P-rich layer and the consumed Co(W,P) film versus the square root of aging time.

that the thickness of the P-rich layer remained unchanged after prolonged aging. Figure 2c summarizes the thicknesses of the P-rich layer and the consumed Co(W,P) as a function of the square root of time. Although the P-rich layer does not thicken during the prolonged aging, there is no ceasing of Co(W,P) consumption. The plot shown in Fig. 2c reveals that this layer did not inhibit further alloy reactions. Subsequent TEM analysis revealed that the P-rich layer is polycrystalline, comprised of nanoscale IMCs. It is therefore speculated that fine IMCs continuously detach from the P-rich interfacial layer into the molten solder, while the IMCs unceasingly form as the Sn diffuses through the P-rich layer to react with Co(W,P).

XTEM analysis was carried out to explore the detailed microstructure and composition changes at the SnBi/Co(W,P) interface, and the analytical results for the sample subjected to 1 h liquid-state aging are presented in Fig. 3. The polycrystalline nature of the P-rich layer is identified by the inset selected-area electron diffraction (SAED) pattern, which reveals various IMC types, e.g., Co_3Sn_2, CoSn, CoP, and SnP_3. Furthermore, the absence of a distinctive granular contrast in the P-rich layer

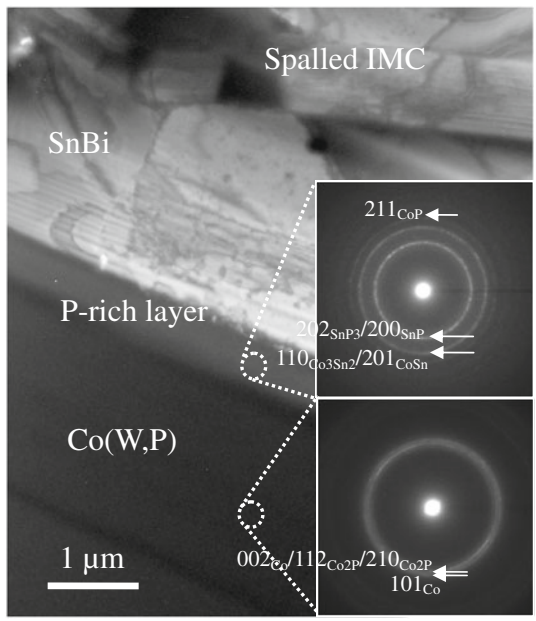

Fig. 3. XTEM image of SnBi/amorphous Co(W,P) subjected to liquid-state aging for 60 min. SAED patterns taken from P-rich layer and unreacted Co(W,P) (indicated by broken circles) are inset on the right of the micrograph.

implies extremely small IMC sizes. It is speculated that the accumulated P and W inhibit grain coarsening during IMC formation and result in the fine IMC mixture in the P-rich layer.

A SAED pattern taken from the unreacted Co(W,P) region is also presented in Fig. 3. Careful examination of the diffraction pattern revealed that the amorphous Co(W,P) tends to recrystallize due to the high-temperature liquid-state aging and Co_2P IMCs emerge due to the supersaturated P content in Co(W,P). Grain boundaries in a polycrystalline layer may form short-circuit diffusion paths. However, the content of Sn and Cu in the unreacted Co(W,P) is negligible, as illustrated by the EDS line scan profiles shown in Fig. 1e. It is believed that the supersaturated P and Co_2P IMCs may segregate into the grain boundaries of the recrystallized Co(W,P) to block the elemental diffusion. This confirms the mixed-type, i.e., sacrificial- plus stuffed-type, diffusion barrier behavior of amorphous Co(W,P) in the SnBi/amorphous Co(W,P)/Cu diffusion couple.

Solid-State Aging

Figure 4a and b, respectively, present the SnBi/amorphous Co(W,P) samples subjected to solid-state aging for 1000 h together with their corresponding EDS line scan profiles. $CoSn_3$ IMC clusters neighboring a ~300-nm-thick P-rich layer (P content of ~12 at.% and W content of ~1.8 at.%) were observed, as shown in Fig. 4a. The comparatively thinner P-rich layer is ascribed to the low solid-state aging temperature of 120°C in comparison with the liquid-state aging temperature of 250°C. The EDS line scan profiles shown in Fig. 4b imply a similar barrier behavior as presented in the previous section; i.e., the formation of IMCs indicates sacrificial-type barrier characteristics, while the high P content in Co(W,P) might provide evidence for stuffed-type barrier behavior.

An XTEM image corresponding to the sample shown in Fig. 4a is shown in Fig. 5a, in which the lath-like IMCs and P-rich layer can be seen more clearly. Owing to the low solid-state aging temperature, the P-rich layer is more prone to be nanocrystalline, as indicated by the broad concentric diffraction rings in the SAED pattern shown in Fig. 5a. Figure 5b presents an XTEM image and SAED patterns taken from different portions of the unreacted Co(W,P). It can be seen from Fig. 5b that the solid-state aging temperature was too low to induce any substantial recrystallization in Co(W,P). The mainly amorphous structure in Co(W,P) seems to imply amorphous-type barrier behavior according to the usual classification schemes.[1] Nevertheless, subsequent analysis of polycrystalline Co(W,P) samples indicated that it is debatable whether structural amorphism can be correlated with barrier capability. Although the high P content is the cause of the amorphism, supersaturated P plays

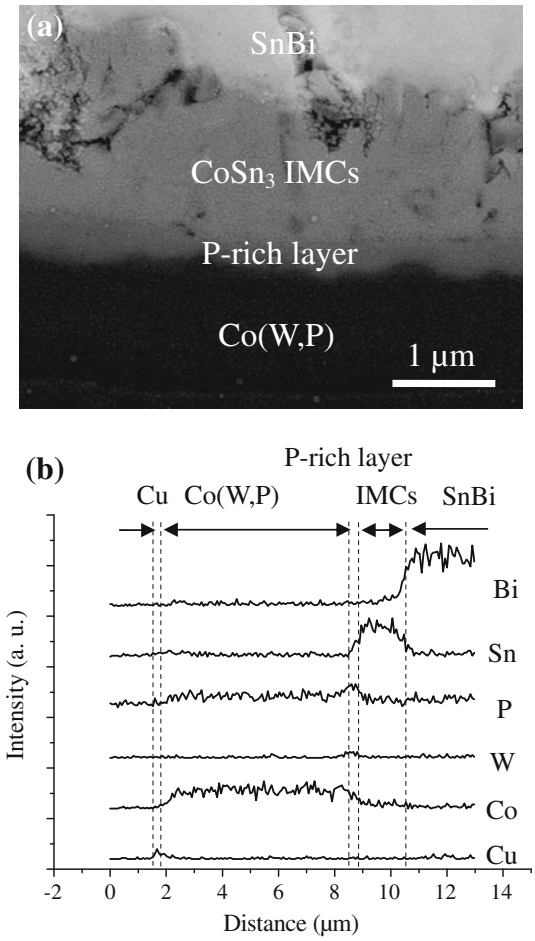

Fig. 4. (a) SEM micrograph of SnBi/amorphous Co(W,P) sample subjected to solid-state aging for 1000 h, and (b) corresponding EDS line scan profiles.

a dominant role in inhibiting interdiffusion in the unreacted Co(W,P). Hence, in the case of SnBi/amorphous Co(W,P) couples subjected to solid-state aging, Co(W,P) remains a sacrificial- plus stuffed-type barrier rather than a sacrificial- plus amorphous-type barrier.

SnBi/Polycrystalline Co(W,P) Samples

Liquid-State Aging

Figure 6a–c, respectively, present cross-sectional SEM views for a SnBi/polycrystalline Co(W,P) couple subjected to liquid-state aging for 1 h, 2 h, and 5 h. EDS line scan profiles corresponding to the sample couple subjected to 1 h liquid-state aging are depicted in Fig. 6d. Unlike amorphous Co(W,P), lath-like $CoSn_3$ IMCs reside at the SnBi/Co(W,P) interface without spallation. SEM micrographs presented in Fig. 6a–c clearly depict that IMCs coarsen with increasing aging time. Continuous growth of IMCs clearly indicates the sacrificial-type barrier behavior of polycrystalline Co(W,P).

Figure 6a–c also reveals a reaction layer between the IMCs and the Co(W,P) film. This reaction layer,

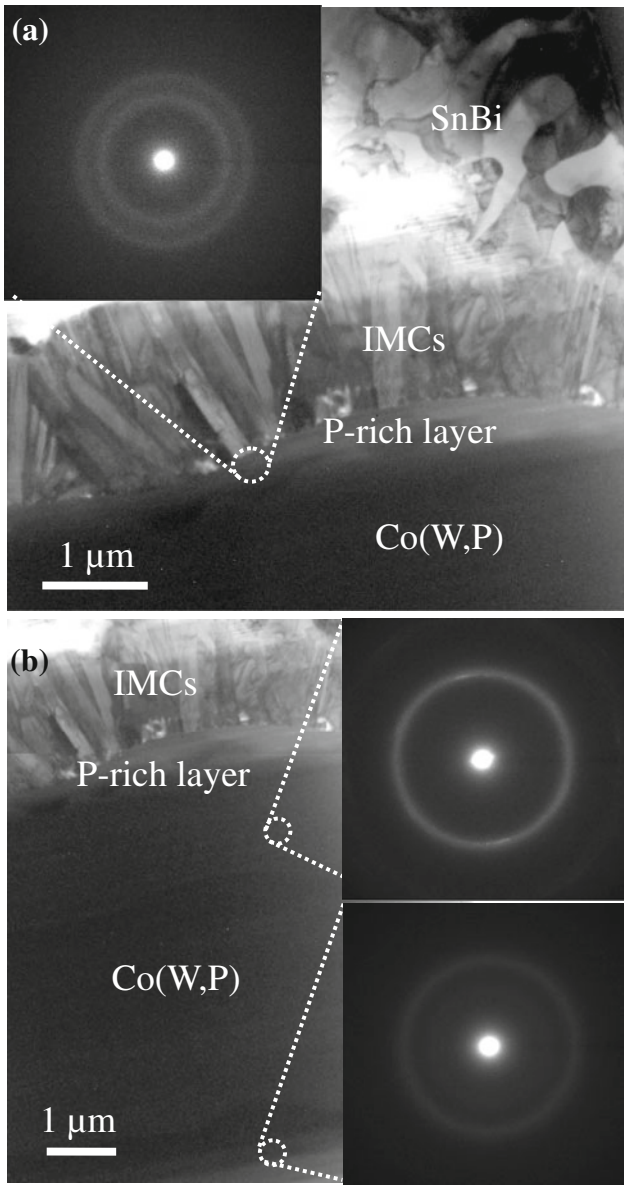

Fig. 5. XTEM images taken from (a) reaction interface and (b) unreacted Co(W,P) in SnBi/amorphous Co(W,P) sample subjected to solid-state aging for 1000 h. Regions subjected to SAED analysis are indicated by broken circles.

in contrast to the P-rich layer observed for amorphous Co(W,P), thickens with increasing aging time. This thickening effect is shown in Fig. 7, which plots the thickness of the reaction layer (termed the W-rich layer due to its relatively high W content as observed by subsequent XTEM analysis) and the consumed Co(W,P) film versus the square root of aging time. The sacrificial nature of the polycrystalline Co(W,P) film is further supported by the plot of consumption of Co(W,P) film versus the square root of aging time, as shown in Fig. 7.

Also apparent from Fig. 7 is that the W-rich layer thickens at a rate faster than the rate of Co(W,P) consumption. The phase diagram for Co-W binary alloys indicates that the solubility of W in Co is extremely low at temperatures below 500°C.[24] Hence, grain boundaries in polycrystalline Co(W,P) are most likely the fast-diffusion paths for migration of P and W toward the reaction interface.

XTEM analysis for a SnBi/polycrystalline Co(W,P) couple subjected to 1 h liquid-state aging is depicted in Fig. 8. SAED, in conjunction with EDS analysis, shows the reaction layer to be amorphous (see the SAED pattern inset in Fig. 8) with a P content of ~6 at.% and a surprisingly high W content of ~15 at.%. Apparently, consumption of Co by Sn to form the IMCs implies accumulation of P and W at the reacting interface; the high W concentration might be due to the low solubility of W in Co and the relatively low P content in polycrystalline Co(W,P). Furthermore, the Co_2P phase and/or the Co-W alloy phase were detected by SAED/EDS analyses in the unreacted polycrystalline Co(W,P) in negligible amounts. This is ascribed to the very low P content in polycrystalline Co(W,P) as well as the loss of W to the reaction interface via grain boundary diffusion. This weakens the role of the stuffed-type barrier mechanism for polycrystalline Co(W,P) film, and therefore we deduce that the Co(W,P) film is mainly a sacrificial-type barrier.

An interesting feature deduced from the above analysis is that, even though the W-rich layer is amorphous, it does not inhibit alloy reactions between the solder and the Co(W,P) film, as illustrated by the continuous growth of IMCs into the solder as shown in Fig. 6a–c. The diffusion barrier characteristics for amorphous films are generally attributed to the absence of fast-diffusion grain boundaries. However, amorphism may also be viewed as a chaotic structure with abundant crystalline defects which are essential for bulk diffusion. In conjunction with this finding, it seems that structural amorphism does not necessarily lead to a diffusion barrier capability;[1] rather, it is the nature of the chemical bonding that governs the diffusion barrier characteristic of the materials.

Another interesting finding deduced from the above characterizations is the correlation between spallation of IMCs and the P content of the Co(W,P) films. IMCs tend to spall away from the reacting interface for the couple containing an electroless Co layer with high P content. Guo et al. reported that solderability is suppressed in EN due to the presence of phosphide precipitates.[12] Sohn and Yu observed that IMCs spall away from a Ni(P) surface when the P content and reflow time are increased.[13] Furthermore, spallation is a result of surface energy reduction,[25] and therefore, in comparison with chunky-type IMCs, it would be easier for the needle-like IMCs to spall away from the reaction interface due to its high surface-to-volume ratio. In addition to the good agreement with previous studies, our analytical results indicate that the P content in the electroless Co(W,P) layer affects not only its crystallinity but also the structure evolution at

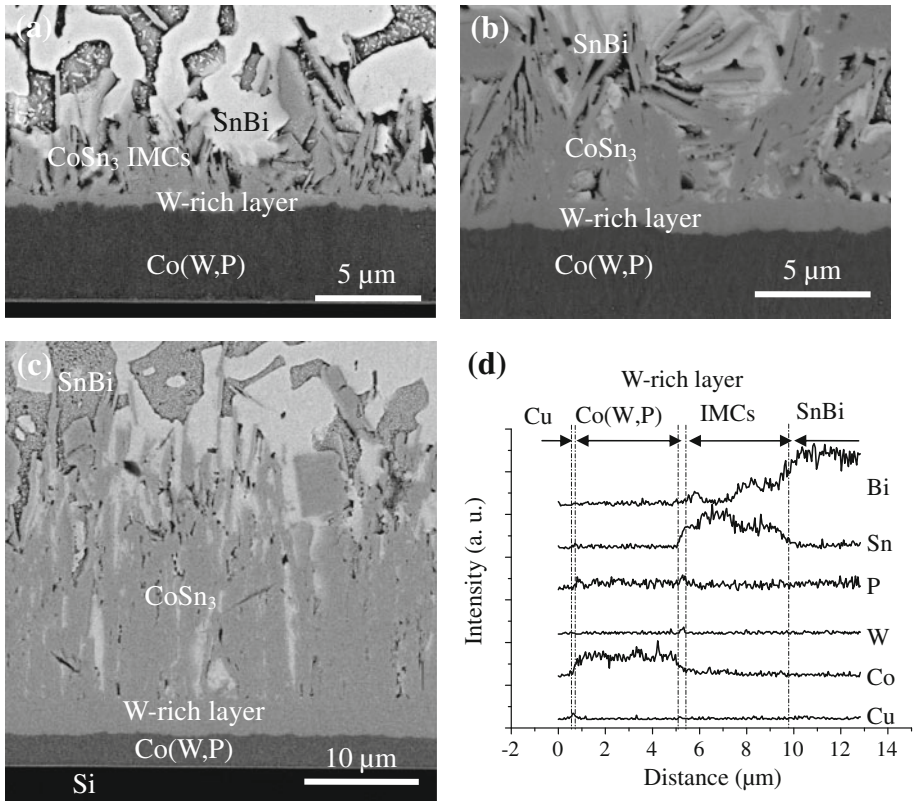

Fig. 6. (a) SEM view of SnBi/polycrystalline Co(W,P) samples subjected to liquid-state aging for (a) 1 h, (b) 2 h, and (c) 5 h. (d) EDS line scan profiles corresponding to the sample subjected to 1 h liquid-state aging.

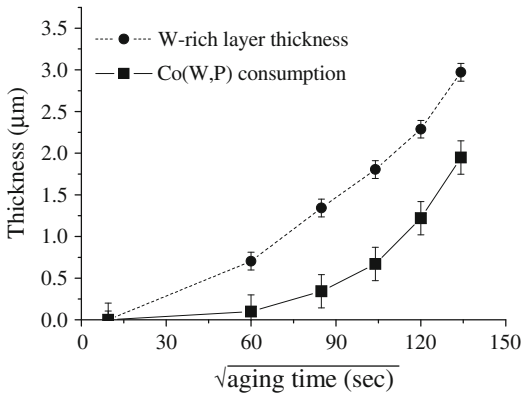

Fig. 7. Plot of consumption of Co(W,P) layer and W-rich layer thickness versus the square root of aging time in SnBi/polycrystalline Co(W,P) samples subjected to liquid-state aging.

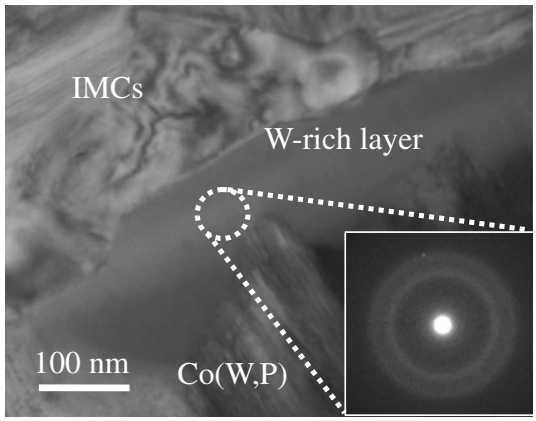

Fig. 8. XTEM micrograph of reaction layer in SnBi/polycrystalline Co(W,P) subjected to liquid-state aging for 1 h. Inset SAED pattern taken in the vicinity of the reaction layer.

the reacting interface and the diffusion barrier mechanism.

Solid-State Aging

Cross-sectional SEM views of SnBi/polycrystalline Co(W,P) couples subjected to solid-state aging for 1000 h and corresponding EDS line scan profiles are presented in Fig. 9a and b, respectively. Thick, lath-like IMCs can be seen, and according to EDS analysis, they are mainly $CoSn_3$. The average IMC thickness is less than that observed in the couples subjected to liquid-state aging due to the lower solid-state aging temperature. This also leads to a thinner W-rich layer, so that the SEM can barely reveal its existence. SEM characterizations of the samples aged for various times also showed that IMCs thicken with increasing aging time, implying that the polycrystalline Co(W,P) is mainly a sacrificial-type barrier.

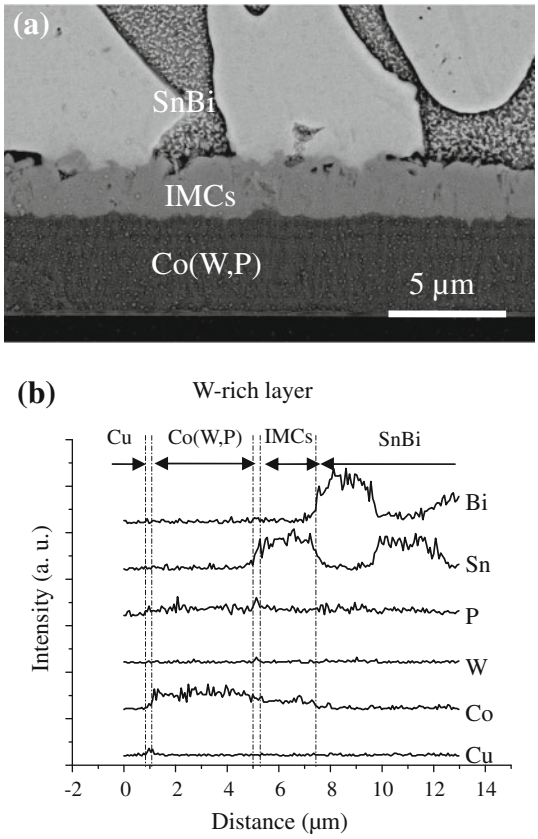

Fig. 9. (a) Cross-sectional SEM view of SnBi/polycrystalline Co(W,P) subjected to solid-state aging for 1000 h, and (b) the corresponding EDS line scan profiles.

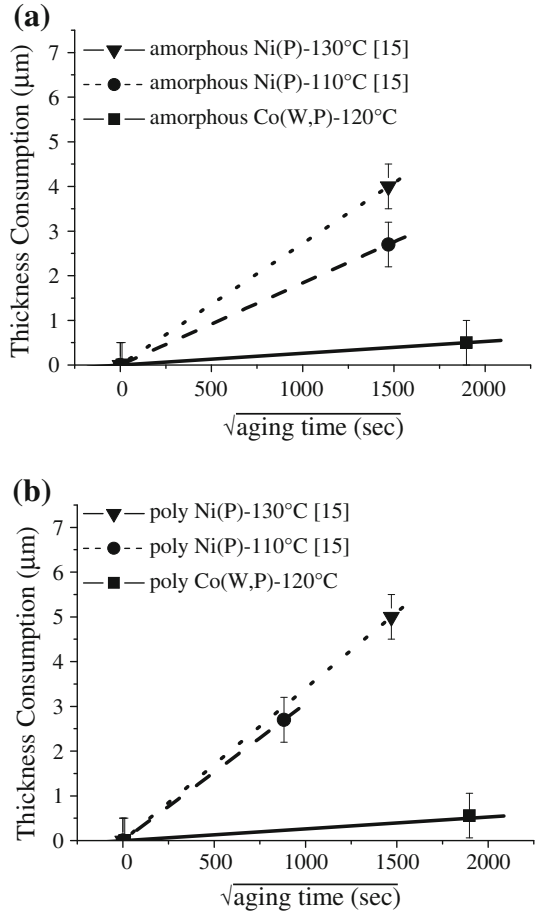

Fig. 10. Thickness consumption of (a) amorphous Co(W,P) and EN and (b) polycrystalline Co(W,P) and EN versus the square root of time.

Comparison of Barrier Capabilities of Electroless Co(W,P) and EN Layers

Alloy reactions between SnBi solder and EN with different crystallinities at 110°C and 130°C have been reported by Young et al.[15] Since their aging temperatures are quite close to our solid-state aging temperature, a comparison is made to explore the barrier properties for EN and electroless Co(W,P) films. Figure 10a and b, respectively, present the thickness consumption data for Co(W,P) and EN layers. The data show that electroless Co(W,P) films have lower consumption rates regardless of crystallinity. IMC thickness versus the square root of aging time for SnBi/Co(W,P) and SnBi/EN couples with different crystallinities are plotted in Fig. 11a, b. The data show a slower IMC growth rate for electroless Co(W,P). Hence, electroless Co(W,P) is expected to be a better diffusion barrier to solder in comparison with EN.

It is expected that amorphous Co(W,P) film is a better diffusion barrier than crystalline Co(W,P) film due to its mixed-type barrier characteristic. Furthermore, since IMCs are generally brittle, spallation might eliminate their bulk accumulation at the solder/Co(W,P) interface and benefit solder joint mechanical reliability. Nevertheless, amorphous Co(W,P) remains a sacrificial-type diffusion barrier that will react with solder during a reflow or soldering process. A sufficiently thick Co(W,P) layer (at least 1 μm for SnBi-related applications, estimated based on the above characterizations) is therefore required to avoid total consumption of the barrier structure that may lead to degradation of joint reliability.

CONCLUSIONS

Amorphous and polycrystalline electroless Co(W,P) layers were prepared and their diffusion barrier properties relative to lead-free SnBi solder were investigated in this study. For the SnBi/amorphous Co(W,P) couple subjected to liquid-state aging, the lath-like $CoSn_3$-type IMCs spalled into the SnBi solder and formation of a P-rich layer at the SnBi/Co(W,P) interface was observed. The P-rich layer was formed by P accumulation during the SnBi/Co(W,P) interaction. This layer is a polycrystalline layer intermixed with various IMCs in nanometer scale. Due to the higher liquid-state aging temperatures, amorphous Co(W,P) tends to recrystallize and Co_2P IMCs are formed due to the supersaturated P content in the Co(W,P) layer (as

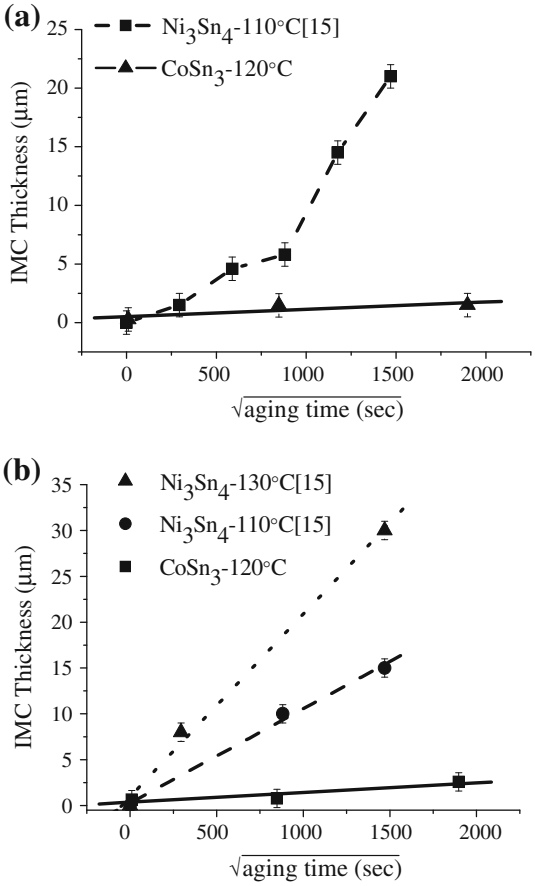

Fig. 11. Variation of IMC thickness with the square root of time for (a) amorphous Co(W,P) and EN and (b) polycrystalline Co(W,P) and EN.

revealed by XTEM). No spallation of IMCs from the P-rich layer was observed for SnBi/amorphous Co(W,P) couples subjected to solid-state aging. According to the compositional analysis, amorphous Co(W,P) serves as a mixed-type, i.e., sacrificial- plus stuffed-type, diffusion barrier.

For the SnBi/polycrystalline Co(W,P) couples subjected to both aging treatments, $CoSn_3$ IMCs adjacent to a W-enriched amorphous layer were observed at the reaction interface. Analytical results indicated that the polycrystalline Co(W,P) is essentially a sacrificial-type barrier to the SnBi solder. An interesting finding was that the presence of the amorphous W-rich layer does not inhibit subsequent alloy reactions. It is, therefore, the nature of chemical bonding that is primarily responsible for the nature of the diffusion barrier, rather than the structural amorphism. In addition, it was found that the P content in the electroless Co(W,P) film also affects the structural evolution at the reacting interface and the diffusion inhibition mechanism. A comparison between the Co(W,P) film consumption rate and the IMC formation rate shows that the diffusion barrier capability of the electroless Co(W,P) is better than that of EN, and that amorphous Co(W,P) exhibits better diffusion barrier characteristics than does polycrystalline Co(W,P).

ACKNOWLEDGEMENTS

This study is supported by the National Science Council (NSC), Taiwan, R.O.C., under Contract No. NSC-96-2221-E-009-010. SEM analysis is supported by the Biomedical Detection Technology Division, Medical Electronics and Devices Technology Center, Industrial Technology Research Institute (ITRI), Hsinchu, Taiwan, R.O.C., and FIB/TEM/EDS analyses are supported by Materials Analysis Technology, Inc., Chupei, Taiwan, R.O.C., which are also deeply appreciated.

REFERENCES

1. M.A. Nicolet, *Thin Solid Films* 52, 415 (1978).
2. D.R. Frear, F.M. Hosking, and P.T. Vianco, *Proceedings Materials Developments in Microelectronic Packaging Conference* (Materials Park, OH: ASM International, 1991), pp. 229–240.
3. R.H. Uang, K.C. Chen, S.W. Lu, H.T. Hu, and S.H. Huang, *Proceedings of 3rd IEEE Electronic Packaging Technology Conference, Singapore, December 5–7*, ed. L.T. Beng, C. Lee, and T.K. Chuan (EPTC, 2000), p. 292.
4. M.W. Liang, T.E. Hsieh, C.C. Chen, and Y.T. Hung, *Jpn. J. Appl. Phys.* 43, 8258 (2004).
5. T. Oppert, E. Zakel, and T. Teutsch, *Proceedings of the International Electronics Manufacturing Technology Symposium (IEMT) Symposium, Omiya, Japan, April 15–17, 1998*, *Proceedings of 2nd IEMT/IMC Symposium* (Omiya, 1998), p. 106.
6. T. Teutsch, T. Oppert, E. Zakel, and E. Klusmann, *Electronic Component and Technology Conference* (Las Vegas, NV, USA: IEEE, 2000), p. 107.
7. G.O. Mallory and J.B. Hajdu, *Electroless Plating Fundamentals and Applications*, Chap. 1–7 (Florida: AESF Orlando, 1990).
8. M.S. Lee, C. Chen, and C.R. Kao, *Chem. Mater.* 11, 292 (1999).
9. M.S. Lee, C.M. Liu, and C.R. Kao, *J. Electron. Mater.* 28, 57 (1999).
10. W.H. Tao, C. Chen, C.E. Ho, W.T. Chen, and C.R. Kao, *Chem. Mater.* 13, 1051 (2001).
11. B.L. Young and J.G. Duh, *J. Electron. Mater.* 30, 878 (2001).
12. J.J. Guo, A.P. Xian, and J.K. Shang, *Surf. Coat. Technol.* 202, 268 (2007).
13. Y.C. Sohn and J. Yu, *J. Mater. Res.* 19, 2428 (2004).
14. J. Wang, H.S. Liu, L.B. Liu, and Z.P. Jin, *J. Electron. Mater.* 35, 1842 (2006).
15. B.L. Young, J.G. Duh, and G.Y. Jang, *J. Electron. Mater.* 32, 1463 (2003).
16. J.I. Lee, S.W. Chen, H.Y. Chang, and C.M. Chen, *J. Electron. Mater.* 32, 117 (2003).
17. C.Y. Lin, C.C. Jao, C. Lee, and Y.W. Yen, *J. Alloys Compd.* 440, 333 (2007).
18. J.F. Li, S.H. Mannan, M.P. Clode, K. Chen, D.C. Whalley, C. Liu, and D.A. Hutt, *Acta Mater.* 55, 737 (2007).
19. E.J. O'Sullivan, A.G. Schrott, M. Paunovic, C.J. Sambucetti, J.R. Marino, P.J. Bailey, S. Kaja, and K.W. Semkow, *IBM J. Res. Dev.* 42, 607 (1998).
20. M.W. Liang, H.T. Yen, and T.E. Hsieh, *J. Electron. Mater.* 35, 1593 (2006).
21. A. Kohn, M. Eizenberg, Y. Shacham-Diamand, and Y. Sverdlov, *Mater. Sci. Eng.* A302, 18 (2001).

22. A. Kohn, M. Eizenberg, Y. Shacham-Diamand, B. Israel, and Y. Sverdlov, *Microelectron. Eng.* 55, 297 (2001).
23. W.C. Wu, T.E. Hsieh, and H.C. Pan, *J. Electrochem. Soc.* 155, D369 (2008).
24. T.B. Massalski, *Binary Alloy Phase Diagrams*, 2nd ed. (Materials Park, OH: ASM International, 1990).
25. J.W. Jang, L.N. Ramanathan, J.K. Lin, and D.R. Frear, *J. Appl. Phys.* 95, 8286 (2004).